Iran University of Science and Technology

Automotive Science and Engineering

Journal Homepage: ase.iust.ac.ir

ISSN: 2008-9899

Thermo-elastic stress assessment of exhaust manifold outlet dimensional deviations in a heavy-duty diesel engine

Mohammad Parhizkar Yaghoobi[1*], Emad Rajabi[2]

[1, 2] MAPNA Turbine Engineering and Manufacturing Company (TUGA), MAPNA Group, Tehran, Iran

ARTICLE INFO

Article history:

Received : 23 Jul 2025

Accepted: 4 Feb 2026

Published: 19 Feb 2026

Keywords:

Exhaust Manifold

Heavy-duty Diesel Engine

Thermo-Elastic Stress

Computational Fluid Dynamics (CFD)

Finite Element Analysis (FEA)

A B S T R A C T

Generally, parts whose geometric form in the final configuration, or before additional operations such as machining, does not require special dimensional accuracy are produced using casting methods. Producing parts with this method results in significant deviations in dimensions and geometric forms from the main designed geometric model. Due to economic considerations, scrapping such parts will result in energy and material waste and high costs. In this study, dimensional deviations at the exhaust manifold outlet and deviations from the defined geometric tolerance limits of the part during the repair process are identified as geometric non-conformities and investigated using computer tools. Considering the harsh operating conditions under which the engine is under full load, the temperature distribution is determined using computational fluid dynamics, and the thermo-elastic stress distribution is calculated using the finite element method, accounting for the loads applied to the structure. The main part model and the non-conforming models with upper and lower limits in geometric dimensions have been investigated with respect to the deviation in thermo-elastic stress relative to the reference value in the part with the nominal size. The results showed that, given the amount of stress changes in the desired area of parts with deviations from the main design, these parts are also usable and have a lifetime almost the same as a part produced with the nominal size.

1. Introduction

The exhaust manifold, mounted to the engine cylinder head with bolts, collects the hot exhaust gases from the cylinders and directs them to the engine's exhaust system. In certain applications, this component may experience exhaust gas temperatures exceeding 1000 °C. The elevated temperature induces thermal expansion in the manifold; due to constraints at the cylinder head and turbocharger connection, thermal strains and stresses develop within the component. Furthermore, the engine operates over a wide temperature range, from ambient conditions to full-load operation, which subjects the manifold to cyclic thermal loading. Such loading can lead to thermomechanical fatigue failure of the exhaust manifold. Therefore, this component must possess sufficient strength to withstand the varying thermal cycles encountered during engine operation, including start-up, steady-state warming, and full-load combustion. In fact, the exhaust manifold experiences a transient, non-

*Corresponding Author
Email Address: m.parhizkaryaghoobi@gmail.com; parhizkar.mohammad@tuga.mapnagroup.com;
http://doi.org/10.22068/ase.2026.732

"*Automotive Science and Engineering*" is licensed under a Creative Commons Attribution-Noncommercial 4.0 International License.

[Downloaded from rds.iust.ac.ir on 2026-11-15]

[DOI: 10.22068/ase.2026.732]

uniform temperature field coupled with assembly-induced constraint loads [1–3]. The main mechanism of failure in exhaust manifolds is thermomechanical fatigue, which, depending on the experienced environmental and thermal conditions, may be collaborated by creep and, occasionally, oxidation [4–5].

Approximately, casting alloys used in the hot section of engines can be classified into four categories based on the exhaust gas temperature, as shown in Figure 1. The general criteria for material selection include castability, cost-effectiveness, low weight, chemical corrosion resistance, and desirable mechanical properties at elevated temperatures. Additionally, low thermal expansion coefficients and high thermal conductivity lead to lower thermal strains and, consequently, reduced thermal stresses in constrained regions, making physical properties critical for components in the engine hot section [6–7].

The most common and widely used material for exhaust manifolds is ferritic ductile cast iron. This material is preferred for its excellent castability (low melting point), which reduces production costs. Silicon-molybdenum alloys of this category are typically employed for diesel engines with exhaust gas temperatures up to 750 °C [8–9].

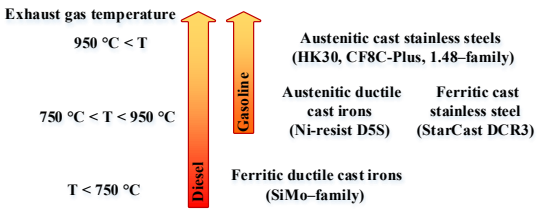


Figure 1: Classification of common casting alloys in exhaust manifold production

At higher temperatures, austenitic ductile cast irons, which are more expensive and commercially known as Ni-Resist D5S, are generally used in gasoline engines. These alloys maintain favourable mechanical properties up to 850 °C. Another category includes ferritic stainless steel casting alloys, which offer superior high-temperature mechanical properties and enhanced chemical corrosion resistance compared to the previous two categories. However, the presence of coarse carbon particles in their microstructure may be detrimental to fatigue life. These alloys are commonly used in the form of formed sheets for gasoline engine exhaust manifolds exposed to exhaust temperatures up to 900 °C [9].

The most advanced technology involves austenitic stainless steel castings, employed when the previous material groups reach their application limits. These alloys can be used in exhaust manifolds exposed to exhaust gas temperatures around 1000 °C [10]. It is worth mentioning that under the harsh operational conditions, these alloys may experience short-term thermal exposures above their nominal classification temperature. Also, it is important to note that engine components generally experience variable-amplitude loading during their service life. Conducting experimental tests under these realistic loading histories is challenging and complicates the correlation of experimental and computational results. In such cases, fatigue tests with variable-amplitude loading are conducted in accordance with standards such as ASTM E1049-85 and ISO 12110, based on the component's actual loading history. Designers can then evaluate the correlation between experimental results and computational models.

Höschler et al. (2002) performed a thermomechanical analysis of a diesel engine exhaust manifold [11]. Their study detailed a thermomechanical method that emphasised accurate modelling of transient heat transfer in the hot gas section, coupling a one-dimensional gas-flow analysis with a three-dimensional thermal finite-element analysis. The effect of operating characteristics of a four-stroke diesel engine on local heat transfer was considered using appropriate correction factors, and the influence of transients on stress distribution in the manifold was investigated. Delprete et al. (2010) [12] compared conventional and novel thermomechanical analyses of a cast iron manifold. In the conventional approach, thermal analysis provided the temperature field, which was then used in mechanical stress analysis. To investigate the interaction between thermal and

[Downloaded from rds.iust.ac.ir on 2026-11-15]

[DOI: 10.22068/ase.2026.732]

mechanical fields, a multiphysics approach based on the cell method was proposed, enabling time-dependent thermomechanical analysis of a virtual manifold.

In 2014, Rajadurai et al. [13] investigated the need for modal analysis of exhaust manifolds under high-temperature conditions. Their study highlighted that, due to the elevated temperatures experienced at the hot end of the engine (approximately 800 °C) and the significant effect of temperature on the physical and mechanical properties of the manifold and hot-end components, it is necessary to evaluate not only structural integrity but also the impact on vibrational characteristics.

Parallel to studies on hot-section components and exhaust manifolds, materials scientists have characterised and modelled the behaviour of materials used in these components. Yang et al. [14] determined crack properties and thermal fatigue behaviour for high-silicon, high-molybdenum spheroidal graphite cast iron. Ohmenhäuser et al. [15] performed structural modelling for thermomechanical fatigue and lifetime prediction of austenitic stainless cast steel (1.4849). Mao et al. [16] conducted a comparative evaluation of elasto-viscoplastic models for thermal stress analysis of exhaust manifolds, using two locally developed models calibrated with standard experimental data. The Chaboche model showed higher computational efficiency than the Sehitoglu model.

Vyas et al. (2015) [17] performed multiphysics simulations for a six-cylinder diesel engine exhaust manifold, determining temperature distributions using computational fluid dynamics (CFD) and subsequently mapping them onto finite element nodes for thermomechanical stress evaluation. In 2016, Eroglu et al. [18] applied CFD-FEA coupling to predict thermomechanical fatigue in a heavy-duty diesel engine manifold, solving convective heat transfer in the fluid, determining temperature distribution, and then extracting structural deformations and fatigue-induced failure. Chen et al. [19] predicted thermomechanical fatigue in an aluminium manifold integrated with a turbocharged gasoline engine, considering elasto-viscoplastic behaviour and experimentally calibrated damage models, with endurance validated by thermal shock tests. Cardoso and Andreatta [20] used one-dimensional analysis, experimentally validated, to determine the temperature distribution and the low-cycle fatigue thermomechanical behaviour in a diesel engine manifold.

In 2018, Liu et al. [21] evaluated thermomechanical fatigue in a ductile cast iron manifold, experimentally determining essential properties and re-evaluating material model variables for fatigue life prediction using a silicon-molybdenum cast iron. Despite ferritic cast iron not meeting certain model requirements due to inter-granular embrittlement at 400 °C, low ductility at low temperatures, and phase transformation between 820–850 °C, the thermomechanical fatigue predictions correlated well with dynamometer durability tests. Celickten et al. [22] optimised convective heat transfer coefficients around a manifold to evaluate and predict temperature distribution, validating the results across similar engine operating conditions.

In 2022, Ramesh Kumar et al. [23] conducted a CFD-based vibrational analysis of a composite diesel engine manifold to identify critical stress and fluid-flow regions. Li et al. [24] investigated manifold failure in a diesel engine after 700 hours of operation, identifying stress concentration and manufacturing defects as primary causes of failure. Chen et al. [25] analysed failure in a natural-gas engine manifold, finding that thermal stresses exceeded the elastic limit and plastic deformation during thermal shock led to structural changes and shrinkage pore formation, causing high-cycle fatigue failure. Structural or material improvements were proposed to prevent failure. In 2025, Jeong et al. [26] evaluated thermomechanical fatigue in ferritic stainless steel (STS444LM) for exhaust manifold applications. Isothermal tensile and low-cycle fatigue tests conducted at 250 to 850-950 °C determined cyclic material properties, and a Morrow-based energy model accounted for peak-temperature effects and dwell time.

As evidenced by the literature reviewed, the exhaust manifold has attracted considerable attention in internal combustion engine research due to its critical role and the diverse challenges

[Downloaded from rds.iust.ac.ir on 2026-11-15]

[DOI: 10.22068/ase.2026.732]

it presents across failure analysis, material modelling, and theoretical studies. In this paper, the effects of thickness variations in the outlet throat of an exhaust manifold for a diesel engine under operation and maintenance by MAPNA Group, rated at 2.4 MW, are investigated. CFD is first used to estimate the non-uniform steady-state temperature under harsh operating conditions. Based on the predicted temperatures and material properties (austenitic ductile cast iron), the dominant failure mechanism is considered thermomechanical fatigue, followed by creep and oxidation. Thermomechanical stresses due to temperature, assembly forces, and combustion gas pressure are calculated using finite element analysis for both the nominal and deviated components. The stress results in the outlet throat region are then compared to assess the acceptability of components with deviations in the repair process.

2. Geometric Model

Figure 2 shows the geometric model of the main exhaust manifold designed for the aforementioned diesel engine, which is made of austenitic ductile cast iron (EN-GJSA-XNiSiCr35-5-2).

Some of the cast components produced have a thickness lower than the nominal value specified for the throat region of the exhaust manifold. Assessment of the produced parts indicates a minimum thickness of 1.5 mm, which deviates by approximately 4 mm from the nominal thickness. Also, parts with a thickness less than 1.5 mm cannot be machined due to a lack of control over the machining tool's vibrations and the resulting final geometry, and should be considered production waste.

Considering the quantity of deviated parts in production, the components are classified into two categories: 1) Minimum thickness between 1.5 mm and 3 mm; 2) Minimum thickness between 3 mm and 5.4 mm. Subsequently, an assembly geometric model, as shown in Figure 3, is prepared for these two categories, with minimum throat thicknesses of 1.5 mm and 3 mm, as well as for the nominal component, and their analysis is conducted accordingly. It is noteworthy that the assembly bolts are carbon steel with a coating, while the cylinder head (mounting base) is grey cast iron.

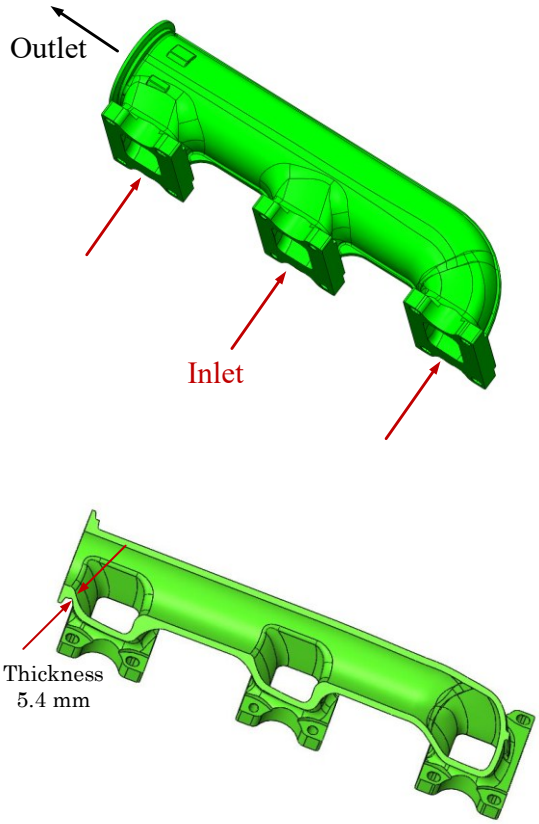


Figure 2: The main geometry of the exhaust manifold

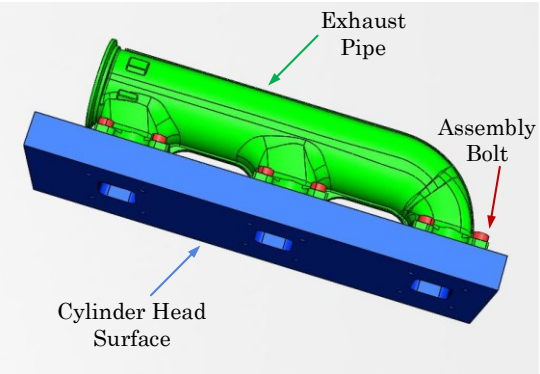


Figure 3: Assembled geometry for thermomechanical analysis of exhaust manifold

[Downloaded from rds.iust.ac.ir on 2026-11-15]

[DOI: 10.22068/ase.2026.732]

3. Thermal Analysis

One of the critical aspects of this component is its thermal loading, as it experiences high, non-uniform temperatures during operation. This loading arises from the passage of hot exhaust gases generated by the combustion in the cylinders. Since exhaust manifold surfaces are generally insulated to increase engine thermal efficiency and to prevent thermal shocks, the component experiences nearly the maximum exhaust gas temperature (Tmax) under steady-state conditions. For design purposes, the engine is evaluated under harsh operating conditions, specifically at full load. Under these conditions, the exhaust gas temperature at the cylinder head reaches 750 °C, with an approximate pressure of 0.4 MPa.

In this study, a computational fluid dynamics (CFD) analysis was performed, and the computational mesh was generated simultaneously for both the gas and solid regions. Consequently, the mesh at the interface between the gas and solid domains is conformal. The mesh was created using ICEM CFD software. Given that the CAD geometry of the exhaust manifold consists of numerous small surfaces, generating a tetrahedral mesh in this type of geometry can result in computational cells with sharp corners and high aspect ratios. To solve this problem, small surfaces can be removed and replaced with larger surfaces, or the edges between surfaces can be removed during mesh generation. Due to the manifold's geometric complexity and high curvature, the first approach would alter the main geometry; therefore, the second approach is employed in this study. The total number of cells in the generated mesh is 4.3 million, of which 2.8 million are in the solid region and 1.5 million are in the gas region.

The heat transfer analysis is performed in a conjugate manner, wherein the heat transfer equations in the solid and fluid domains are coupled at the interface and solved simultaneously. The exhaust manifold geometry is connected to a section of the cylinder head that includes the exhaust gas passage. This section of the cylinder head is approximated as a rectangular block with square cavities corresponding to the inlet ducts to the exhaust manifold (the blue component in Figure 3). Therefore, the computational domain includes three combustion gas inlets to the manifold and one exhaust outlet, as illustrated in Figure 3.

For the CFD simulation, boundary conditions at the manifold inlets are defined as mass flow rates, and at the outlet as pressure. Thermal boundary conditions at the inlets set the exhaust gas temperature to 750 °C, while the manifold walls are assumed adiabatic, which matches the insulated manifold. Even with insulation, some heat is transferred to the outside via heat flux. However, assuming perfect insulation at the exhaust manifold wall allows predicting the maximum temperature that can theoretically occur in the exhaust manifold. This allows the thermoelastic stress to be calculated at its theoretical maximum and for the analysis to be considered under the strict conditions.

The gas is modelled as a homogeneous single-phase mixture with properties averaged from prior combustion simulations. For turbulence modelling, the standard k-ε model is used, with a scalable wall function applied for near-wall flow modelling. Thermal properties of the fluid and the structure used in this analysis are summarised in Table 1.

Table 1: Average thermal properties of the structure and fluid of the assembled exhaust manifold model

Fluid/ Structure	Density (kgm^{-3})	Thermal Conductivity ($Wm^{-1}K^{-1}$)	Specific Heat Capacity ($JK^{-1}kg^{-1}$)	Dynamic Viscosity ($kgm^{-1}s^{-1}$)
Bolt	7.85	45	490	***
Exhaust Manifold	7.45	52	790	***
Cylinder Head	7.25	45	460	***
Outlet Hot Gas	1.48	0.0707	1174	3.7×10^{-5}

[Downloaded from rds.iust.ac.ir on 2026-11-15]

[DOI: 10.22068/ase.2026.732]

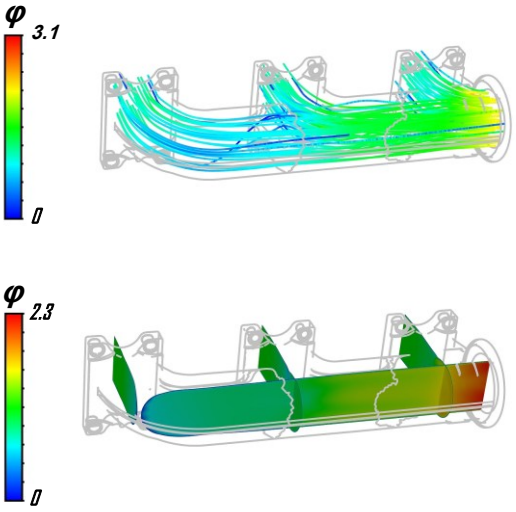


Figure 4: Streamlines and velocity in the main exhaust manifold for hot gas

Figure 4 shows the flow streamlines and the dimensionless velocity distribution of the hot gas inside the main exhaust manifold. In Figure 4, the dimensionless velocity (ϕ) is calculated using (1). In this equation, the gas velocity (V) is non-dimensionalised using the hot gas density (ρ), the mass flow rate at the manifold outlet ($\dot{m}$), and the cross-sectional area of the exhaust manifold outlet (A).

$$\varphi = \frac{\rho A V}{\dot{m}} \quad (1)$$

$$\tau = \frac{T}{T_{max}} \quad (2)$$

Figure 5 shows the distribution of the dimensionless steady-state temperature for the nominal component and the deviated components (with minimum outlet throat thicknesses of 3 mm and 1.5 mm) of the exhaust manifold under severe, harsh operating conditions. In Figure 5, the dimensionless temperature (τ) is calculated using (2), in which the temperature (T) is nondimensionalized by the maximum exhaust gas temperature (T_{max}). As expected, the maximum temperature observed on the exhaust manifold components approaches the maximum exhaust gas temperature, 750 °C (The maximum temperature of the exhaust manifold components reached 99 % of the exhaust gas temperature). As shown, the non-uniform temperature distribution on both the nominal and deviated components is

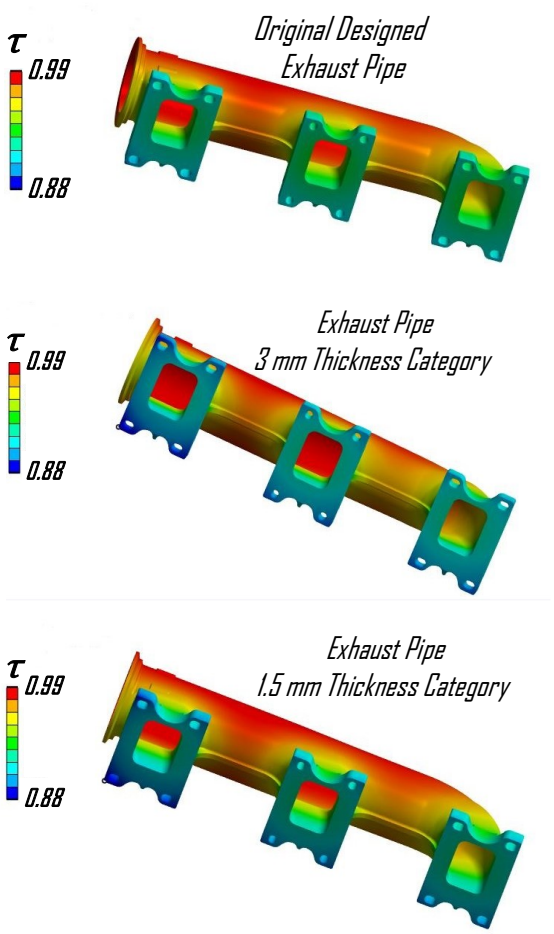


Figure 5: Temperature distribution in the main and non-conformal exhaust manifolds

nearly identical. Hence, in terms of the temperature distribution across the structure, these components can be considered essentially similar.

To assess the thermal analysis results, thermography of the exhaust manifold was performed during operation. The exhaust manifold assembly on the engine is located in a way that prevents direct thermography of this part. A small section of its insulation, which is visible between the two cylinder heads, was thermographed. The thermography results are shown in Figure 6. Thermography on the rock wool insulation (approximately 10 mm thick) covering the exhaust manifold shows a maximum surface temperature of 474 °F (246 °C). Given the insulation layer's thermal resistance, this measurement indirectly confirms an inner wall temperature of approximately 750 °C, consistent

[Downloaded from rds.iust.ac.ir on 2026-11-15]

[DOI: 10.22068/ase.2026.732]



Figure 6: Thermography on the exhaust manifold insulation (temperature in degrees Fahrenheit)

with the CFD result, thereby validating the thermal model.

4. Finite Element Analysis

Due to contact between components, temperature-dependent material properties, and other factors, the problem is inherently nonlinear. Moreover, given the geometric complexity and three-dimensional nature of the problem, it is practically impossible to obtain an analytical solution, necessitating finite element analysis (FEA). Initially, using the thermal distribution in the structure, the strain tensor is calculated based on the coefficient of thermal expansion, accounting for the structural behaviour under applied loads and boundary conditions. Subsequently, stresses in the structure are computed, and the results are compared during post-processing.

For the analysis of any structure, its geometry must first be modelled. However, it should be noted that modelling the entire assembly in full detail results in a complex model that significantly increases computational time and resources for only a minor gain in accuracy. Therefore, the geometry is simplified such that the results remain realistic while the model is not overly complex, and computational demands remain reasonable. Figure 3 shows the exhaust manifold model, including the bolts and a base plate (part of the cylinder head). Contact between the manifold, bolts, and cylinder head is modelled as frictional contact with a coefficient of 0.2 [4, 21], while the bolts themselves are assumed bonded to the cylinder head. The exhaust manifold analysed is made of austenitic ductile iron (EN-GJSA-XNiSiCr35-5-2). After completing the thermal analysis and determining the non-uniform temperature distribution in the component, the material's mechanical and thermal properties at different temperatures are required for the FEA. Figure 7 shows the thermal and mechanical properties of this material at various temperatures, extracted from references [27–28].

For stress analysis using ANSYS software, it is assumed that the inner surface of the exhaust manifold is subjected to the hydrostatic pressure of the exhaust gases from the cylinder. Considering the maximum torque applied to the assembly bolts, a pre-tension of 23,000 N is applied to the bolts. Additionally, due to the assembly configuration, the base plate (cylinder head) is considered fixed, while the manifold outlet is unconstrained.

The computational mesh is generated, and FEA is performed using the mechanical properties of the specified material for the exhaust manifold, bolts, and cylinder head to extract stress results for both nominal and deviated components. It is essential to ensure careful meshing in the FEA model to ensure accurate results and verification.

[Downloaded from rds.iust.ac.ir on 2026-11-15]

[DOI: 10.22068/ase.2026.732]

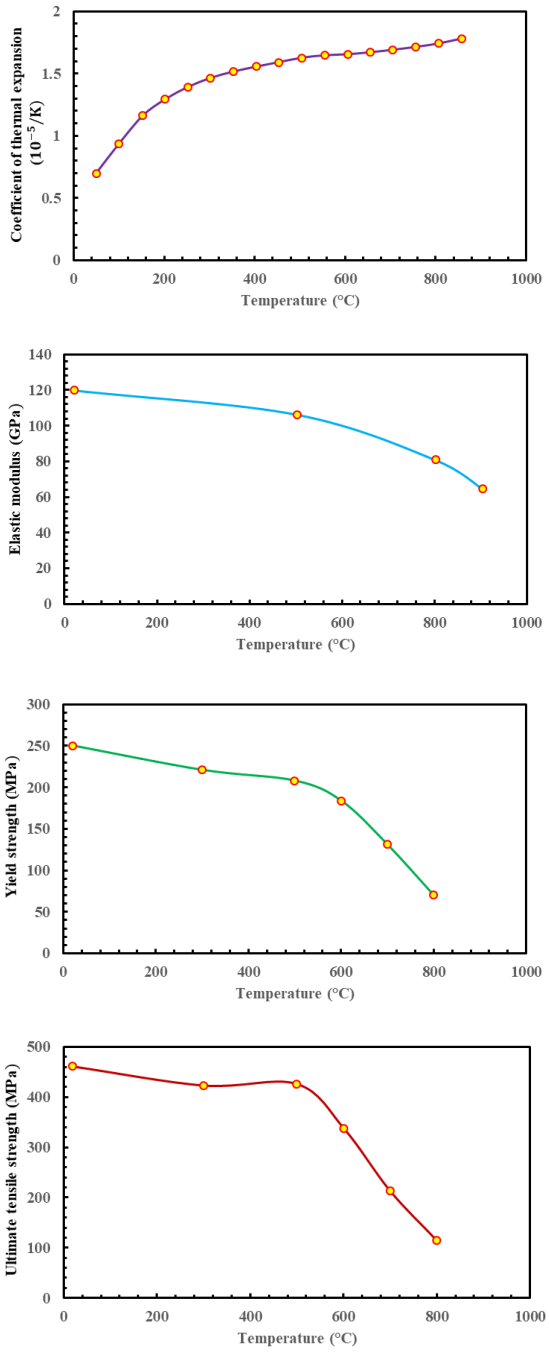


Figure 7: Thermal and mechanical properties of austenitic ductile cast irons (Ni-Resist D5S) at various temperatures

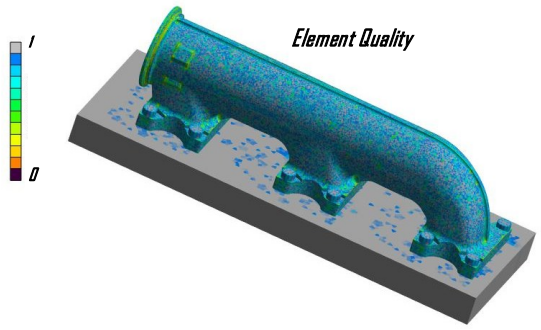


Figure 8: Final quality of assembled computational model elements (best element quality magnitude is one)

Figure 8 illustrates the final mesh quality for the generated elements on the exhaust manifold assembly model. The elements used for the exhaust manifold are tetrahedral, while those for the bolts and the cylinder head are hexahedral. Mesh quality is a mixed metric calculated according to (3) and (4) for tetrahedral and hexahedral elements, respectively. The closer the quality value is to one, the higher the mesh quality. A value of one represents a perfect cube, whereas a value of zero corresponds to an element with no volume. The average quality of the generated elements on the assembly model is 0.8, with a standard deviation of 0.1.

$$Quality = C\frac{Volume}{\sqrt{[\sum(Edge\ Length)^2]^3}} \quad (3)$$

$$C = \begin{cases} 41.57 & For\ Hexagon\ Element \\ 124.71 & For\ Tetrahedron\ Element \end{cases} \quad (4)$$

In addition to ensuring adequate mesh quality across the assembly model, higher-quality elements (with quality values closer to 1) are used in regions of interest, particularly near the exhaust manifold outlet port, to achieve more accurate results. The effect of mesh independence is evaluated in Table 2 for the final mesh configuration. In the third step of the analysis, the results obtained for the assembled model of the main component converge and become independent of the element size. The same

[Downloaded from rds.iust.ac.ir on 2026-11-15]

[DOI: 10.22068/ase.2026.732]

meshing and verification procedure is applied to the models with geometric deviations to ensure the reliability and consistency of the obtained results.

Table 2: The effect of meshing on the analysis result of the main exhaust manifold model

Simulation Iteration	Number of computational mesh nodes	Maximum Von-Mises Stress (MPa)	Maximum Deformation (mm)
1	1732632	257.05	3.61
2	2732736	158.62	3.43
3	5518304	158.61	3.45

Figure 9 illustrates the distribution of the dimensionless equivalent stress (ψ) in the main exhaust manifold, which is calculated using (5). In this equation, the Von Mises stress generated in the structure (σ_{eqv}) is non-dimensionalised using the 0.2% offset yield strength ($Y_{0.2\%@760°C}$) of the material at 760 °C.

$$\psi = \frac{\sigma_{eqv}}{Y_{0.2\%@760°}} \quad (5)$$

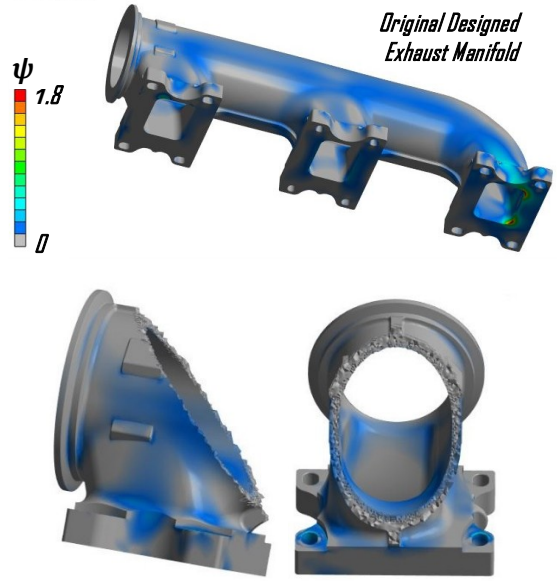


Figure 9: Non-dimensional stress (ψ) in the geometry of the main part

The results of the dimensionless equivalent stress distribution for the main and deviated components (as shown in Figures 10 and 11) are presented for the entire exhaust manifold and its throat region.

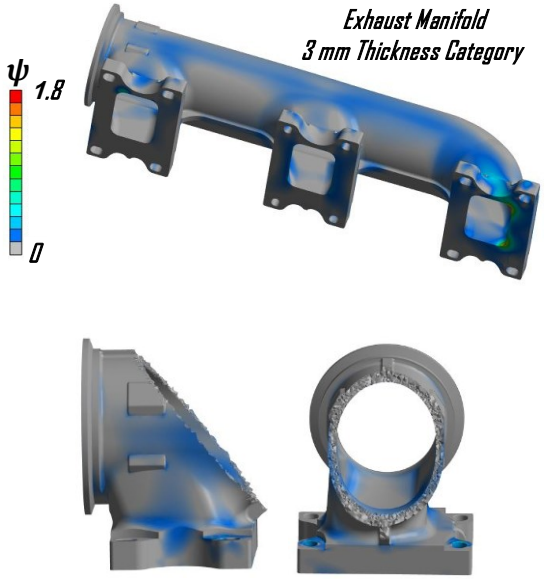


Figure 10: Non-dimensional stress (ψ) in the nonconformal part (minimum outlet thickness 3 mm)

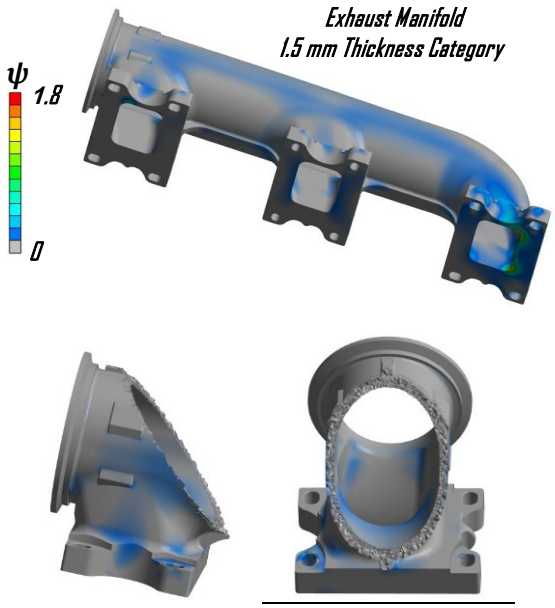


Figure 11: Non-dimensional stress (ψ) in the nonconformal part (minimum outlet thickness 1.5 mm)

[Downloaded from rds.iust.ac.ir on 2026-11-15]

[DOI: 10.22068/ase.2026.732]

The results of the dimensionless equivalent stress distribution for the main and deviated components (as shown in Figures 10 and 11) are presented for the entire exhaust manifold and its throat region.

Table 3 presents the Von Mises stress quantities in the investigated region for the main and deviated components. As observed, the studied region is located away from the critical area of the part (the inlet gas duct), and the average von Mises stress in this region is approximately 8 MPa, which increases up to about twice (16 MPa) at the minimum wall thickness (the focus of this study). Considering that the stress level generated in the investigated area (the exhaust outlet throat region) is far below the 0.2% offset yield strength at 760°C ($Y_{0.2\%@760^\circ}$) and remains nearly the same for both the main and deviated components, this region cannot be considered critical for the exhaust manifold.

According to the general rule of thumb for irons, the endurance limit is approximately 40% of the ultimate tensile strength, with a maximum value of 170 MPa [29]. The maximum von Mises stress in the throat area, according to Table 3, is about 10% of the ultimate tensile strength of the material at a temperature of 750 degrees Celsius. So, it can be concluded that this area is not critical for the part, and, by comparing the stresses in the area under study or the static safety factors, it can be expected that the original part and the parts with deviations will have the same life.

It is also worth noting that, according to laboratory studies, during the service life, the minimum stress level for the activation of creep mechanisms at 750 °C is 18.5 MPa for the material under study [30]. The temperature and stress levels in the area under assessment are lower than those that activate creep mechanisms. In contrast, in other areas, such as the hot gas inlet to the exhaust manifold, the stress levels are high enough to activate the creep mechanism. If these areas are under study, the effect of creep should also be considered in the thermomechanical fatigue failure analysis.

Therefore, these components do not experience yielding and are expected to have nearly identical service lifetimes.

Table 3: Von-Mises stress in the exhaust manifolds outlet (investigation region)

Part	Maximum von-Mises Stress at the minimum outlet thickness (MPa)	Average of von-Mises Stress at the outlet thickness (MPa)
Original Designed Exhaust Manifold	16.25	6.98
Exhaust Manifold 3 mm Thickness Category	15.28	7.43
Exhaust Manifold 1.5 mm Thickness Category	16.08	7.28

Although the average stress variation across the entire exhaust manifold volume between the deviated and main components is about 3%, comparing stress results in critical regions such as the inlet gas duct—where the stress level is close to the yield limit—is not an efficient approach. If this study had focused on those regions, it would have been necessary to perform a thermomechanical fatigue analysis based on strain-based criteria to evaluate the lifetime of the deviated components.

5. Conclusion

In this paper, the effects of geometric variations (thickness reduction) on the thermoelastic stress distribution in the outlet throat region of a heavy-duty diesel engine exhaust manifold were investigated. The studied manifold is a heavy-duty diesel engine operated and maintained by MAPNA Group, which experienced deviations from the nominal wall thickness in the throat region during casting, necessitating repair. The dominant failure mechanism in this component is thermomechanical fatigue (TMF). Therefore, to perform an initial assessment, it was necessary to examine the non-uniform temperature distribution under severe operating conditions and, consequently, the stress distribution due to mechanical and thermal loads. Accordingly,

[Downloaded from rds.iust.ac.ir on 2026-11-15]

[DOI: 10.22068/ase.2026.732]

thermal and thermoelastic stress analyses were performed for both the main and deviated components using Computational Fluid Dynamics (CFD) and the Finite Element Method (FEM). The important findings are summarised as follows:

1. To mesh the solid domain for CFD analysis, due to the geometric complexity and presence of numerous small and curved surfaces, it was not possible to merge small surfaces into larger ones without changing the main geometry. Instead, the shared edges between surfaces were suppressed during mesh generation, allowing the model to be successfully meshed and analysed.

2. The temperature distribution results for the original and deviated components showed that thickness reduction in the outlet throat section had no significant effect on the temperature field, and its influence can be neglected.

3. By employing high-quality meshing, the FEM results for stress and displacement fields achieved mesh independence after at most three computational steps, eliminating the need for further refinement or excessive computation time. It should be noted that the displacement field converged earlier, meaning that, for studies focused on displacement behaviour, computational effort can be significantly reduced by using high-quality meshes.

4. Since the stress range in the outlet throat region for both the main designed and deviated components (considering numerical uncertainty) remained approximately the same and was well below the yield strength at the operating temperature, the outlet throat region is not critical, and no significant difference in service life is expected between the two groups. Therefore, deviated parts can be used by sorting them from thick to thin, provided that monitoring is implemented during operation.

5. If the focus of this research had been on regions near the hot gas inlet, where the stress level approaches the elastic limit, it would have been essential to perform a thermomechanical fatigue analysis using strain-based criteria to compare the service life of the main designed and deviated components and to make informed decisions regarding their usability or scrapping.

References

[1] L. Meda, Y. Shu, M. Romzek, Exhaust System Manifold Development, SAE Technical Paper Series, SAE International, (2012), doi:10.4271/2012-01-0643.

[2] Z. Yan, L. Zhien, X. Wang, H. Zheng, Y. Xu, Cracking Failure Analysis and Optimization on Exhaust Manifold of Engine with CFD-FEA Coupling, SAE International Journal of Passenger Cars - Mechanical Systems, Vol.7, No.2, (2014), pp.873–881, doi:10.4271/2014-01-1710.

[3] R. M. Hazime, S. H. Dropps, D. H. Anderson, M. Y. Ali, Transient Non-linear FEA and TMF Life Estimates of Cast Exhaust Manifolds, SAE Technical Paper Series, SAE International, (2003), doi:10.4271/2003-01-0918.

[4] R. W. Neu, H. Sehitoglu, Thermomechanical fatigue, oxidation, and creep: Part I. Damage mechanisms, Metallurgical Transactions A, Vol.20, No.9, (1989), pp.1755–1767, doi:10.1007/bf02663207.

[5] R. W. Neu, H. Sehitoglu, Thermomechanical fatigue, oxidation, and creep: Part II. Life prediction, Metallurgical Transactions A, Vol.20, No.9, (1989), pp.1769–1783, doi:10.1007/bf02663208.

[6] S. H. Park, J. M. Kim, H. J. Kim, S. J. Ko, H. S. Park, J. D. Lim, Development of a Heat Resistant Cast Iron Alloy for Engine Exhaust Manifolds, SAE Technical Paper Series, SAE International, (2005), doi:10.4271/2005-01-1688.

[7] D. Pierce, J. Smith, K. Johnson, High temperature materials for heavy duty diesel engines: Historical and future trends, Progress in Materials Science, Vol.103, (2019), pp.109–179, doi:10.1016/j.pmatsci.2018.10.004.

[8] M. Ekström, S. Jonsson, High-temperature mechanical- and fatigue properties of cast alloys intended for use in exhaust manifolds, Materials

[Downloaded from rds.iust.ac.ir on 2026-11-15]

[DOI: 10.22068/ase.2026.732]

Science and Engineering A, Vol.616, (2014), pp.78–87, doi:10.1016/j.msea.2014.08.014.

[9] T. Shimamoto, K. Asano, Y. Shioya, S. Ando, Development of the Stainless Cast-Steel Exhaust Manifold, SAE Technical Paper Series, SAE International, (1993), doi:10.4271/930621.

[10] G. Chinouilh, P. O. Santacreu, J. M. Herbelin, Thermal Fatigue Design of Stainless Steel Exhaust Manifolds, SAE Technical Paper Series, SAE International, (2007), doi:10.4271/2007-01-0564.

[11] K. Höschler, J. Bischof, W. Koschel, Thermo-mechanical analysis of an automotive diesel engine exhaust manifold, European Structural Integrity Society, Elsevier, (2002), pp.299–308, doi:10.1016/s1566-1369(02)80086-3.

[12] C. Delprete, C. Rosso, A. Vercelli, Thermo-Mechanical Analysis of a Cast Iron Exhaust Manifold: A Comparison between the Traditional and a New Methodology, SAE Technical Paper Series, SAE International, (2010), doi:10.4271/2010-01-0498.

[13] S. Rajadurai, M. G. Prasad, R. Kavin, M. Sundaravadivelu, Modal Analysis for Exhaust Manifold in Hot Condition, Is There a Need?, SAE Technical Paper Series, SAE International, (2014), doi:10.4271/2014-28-0036.

[14] Y. Yang, Z. Cao, Z. Lian, H. Yu, Thermal Fatigue Behavior and Cracking Characteristics of High Si-Mo Nodular Cast Iron for Exhaust Manifolds, Journal of Iron and Steel Research International, Vol.20, No.6, (2013), pp.52–57, doi:10.1016/s1006-706x(13)60111-9.

[15] F. Ohmenhäuser, C. Schwarz, S. Thalmair, H. S. Evirgen, Constitutive modeling of the thermo-mechanical fatigue and lifetime behavior of the cast steel 1.4849, Materials & Design, Vol.64, (2014), pp.631–639, doi:10.1016/j.matdes.2014.08.016.

[16] J. Mao, C. Engler-Pinto, X. Su, Comparative Assessment of Elastio-Viscoplastic Models for Thermal Stress Analysis of Automotive Powertrain Component, SAE Technical Paper Series, SAE International, (2015), doi:10.4271/2015-01-0533.

[17] S. D. Vyas, A. Patidar, S. K. Kandreegula, U. Gupta, Multi-Physics Simulation of 6-Cylinder Diesel Engine Exhaust Manifold for Investigation of Thermo-Mechanical Stresses, SAE Technical Paper Series, SAE International, (2015), doi:10.4271/2015-26-0182.

[18] S. Eroglu, I. Duman, A. H. Guzel, R. Yilmaz, Durability Analysis of Heavy Duty Engine Exhaust Manifold Using CFD-FE Coupling, SAE Technical Paper Series, SAE International, (2016), doi:10.4271/2016-01-0375.

[19] M. Chen, Y. Wang, W. Wu, Q. Cui, K. Wang, L. Wang, Thermal-Mechanical Fatigue Prediction of Aluminum Cylinder Head with Integrated Exhaust Manifold of a Turbo Charged Gasoline Engine, SAE Technical Paper Series, SAE International, (2016), doi:10.4271/2016-01-1085.

[20] A. de Azevedo Cardoso, E. C. Andreatta, Thermomechanical Analysis of Diesel Engine Exhaust Manifold, SAE Technical Paper Series, SAE International, (2016), doi:10.4271/2016-36-0258.

[21] Y. Liu, J. Zhang, K. Lee, Thermomechanical Fatigue Analysis on a Ductile Cast Iron Exhaust Manifold, SAE International Journal of Materials and Manufacturing, Vol.11, No.4, (2018), pp.517–528, doi:10.4271/2018-01-1215.

[22] B. Celikten, İ. Duman, C. Harman, S. Eroglu, Exhaust Manifold Thermal Assessment with Ambient Heat Transfer Coefficient Optimization, SAE International Journal of Passenger Cars - Mechanical Systems, Vol.11, No.3, (2018), pp.193–202, doi:10.4271/06-11-03-0016.

[23] R. R. Kumar, P. Singh, A. Patel, Vibration analysis of composite exhaust manifold for diesel engine using CFD, Case Studies in Thermal

[Downloaded from rds.iust.ac.ir on 2026-11-15]

[DOI: 10.22068/ase.2026.732]

Engineering, Vol.32, (2022), p.101853, doi:10.1016/j.csite.2022.101853.

[24] Y. Li, J. Liu, W. Huang, Y. Wu, Failure Analysis of a Diesel Engine Exhaust Manifold, International Journal of Metalcasting, Vol.17, No.1, (2022), pp.538–550, doi:10.1007/s40962-022-00796-8.

[25] G. Chen, Y. Hu, S. Yan, J. Zhu, L. Yang, Z. Dong, Failure analysis of a natural gas engine exhaust manifold, Engineering Failure Analysis, Vol.154, (2023), p.107660, doi:10.1016/j.engfailanal.2023.107660.

[26] J.-Y. Jeong, S.-J. Park, D.-C. Ahn, J.-M. Lee, M.-W. Lee, Y.-J. Kim, Thermo-mechanical fatigue analysis of ferritic stainless steel STS444LM for exhaust manifold application, Engineering Failure Analysis, Vol.167, (2025), p.108916, doi:10.1016/j.engfailanal.2024.108916.

[27] M. Ekström, S. Jonsson, High-temperature mechanical- and fatigue properties of cast alloys intended for use in exhaust manifolds, Materials Science and Engineering A, Vol.616, (2014), pp.78–87, doi:10.1016/j.msea.2014.08.014.

[28] C.-H. Hsueh, J. Zhang, L. Chen, Handbook of Mechanics of Materials, Springer, (2019), doi:10.1007/978-981-10-6884-3.

[29] S. Kalpakjian, S.R. Schmid, Manufacturing Engineering and Technology, 7th ed., Pearson, (2013).

[30] C. Öberg, B. Zhu, S. Jonsson, Creep behaviour, creep damage and precipitation in the austenitic ductile cast iron D5S at 750 °C, Materials Science and Engineering: A, Vol.802, (2021), pp.140662, doi:10.1016/j.msea.2020.140662.

[Downloaded from rds.iust.ac.ir on 2026-11-15]

[DOI: 10.22068/ase.2026.732]